COMPARISON BETWEEN SIMULATIONS AND MEASUREMENTS OF HARMONICS IN RESIDUAL EARTH-FAULT CURRENTS OF A 20 KV-NETWORK

Uwe SCHMIDT
TU Dresden – Germany
u.schmidt@tu-dresden.de

Gernot DRUML
Trench Austria – Austria
g.druml@ieee.org

Yu WEI
TU Dresden – Germany
yu.wei28@live.cn

Peter SCHEGNER
TU Dresden - Germany
peter.schegner@tu-dresden.de

ABSTRACT

The resonant-grounding is the dominant neutral point treatment in Germany and Austria for limiting of earth-fault current in distribution systems. Under specific conditions, the harmonic currents can dominate the residual earth-fault current and lead to impermissible values of this current. The determination of residual earth-fault currents is difficult. The theoretical knowledge especially to calculate the harmonics in the residual earth-fault current is insufficient. Therefore currently, the residual earth-fault currents are measured in critical system configurations. Such measurements are cost-intensive and complex. An approach for calculating all components of the residual earth-fault current is introduced considering also harmonic currents in this paper. In this study, the results of the used method are compared with measurements in a 20 kV-network.

INTRODUCTION

In resonant-earthed neutral systems, the star points of the transformers are connected via adjustable inductances (PETERSEN coil[1)]) to the earth. In case of earth faults, the inductive currents $\underline{I}_L$ through the PETERSEN coil compensate the capacitive line-to-earth currents I_{CE}. The principle of the resonant earthing is shown in Figure 1.

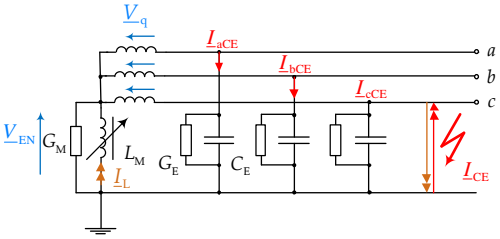

Figure 1: Principle of resonant earthing to compensate the capacitive line-to-earth current I_{CE}

The exact resonant condition between the line-to-earth capacitances and the star point inductance L_M is given in equation (1).

$$3 \cdot \mathrm{j}\omega \cdot L_M = \frac{1}{\mathrm{j}\omega \cdot C_E} \tag{1}$$

The detuning factor v of the resonant circuit is defined to equation (2).

$$v = \frac{I_{CE} - I_L}{I_{CE}} \tag{2}$$

In case of the detuning $v = 0$, the fundamental component of the earth-fault current is only the active residual earth-fault current I_{rw}. The ratio between the active residual earth-fault current I_{rw} and the capacitive line-to-earth current I_{CE} is indicated to the damping d of the system (equation (3)).

$$d = \frac{I_{rw}}{I_{CE}} \tag{3}$$

For detuning $v \neq 0$, the fundamental of residual earth-fault current $I_{res(50)}$ can be determined with equation (4).

$$\begin{aligned} \underline{I}_{res(50)} &= \underline{I}_{CE} \cdot (d + \mathrm{j} \cdot v) \\ I_{res(50)} &= I_{CE} \cdot \sqrt{d^2 + v^2} \end{aligned} \tag{4}$$

Equation (4) descript the 50 Hz-component of the residual earth-fault current I_{res}. In many cases, harmonics dominate the residual earth-fault current I_{res} (PIETZSCH & PRINZ; [1]). For these harmonic currents, the PETERSEN coil is almost ineffective. In this case equation (4) must be extended to relation (5).

$$I_{res} = I_{CE} \cdot \sqrt{d^2 + v^2 + \sum_{\nu} \left(\frac{I_\nu}{I_{CE}} \right)^2} \tag{5}$$

The index ν represents the order of the respective harmonics. The harmonics in the residual earth-fault current I_{res} depend on the loads in the system and on the frequency-dependent impedances. At present, there are different existing methods to estimate the residual earth-fault currents I_{res}. SCHWARZ [2] uses a simple equation to estimate the current harmonics in specific configurations. STADE [3] gives an algorithm to calculate the harmonic earth-fault currents in case of a fault at the main busbar. FISCHER [4] describes an complex and difficult algorithm to estimate the residual earth-fault currents I_{res}.

FREQUENCY-DEPENDENT NETWORK MODELLING

Parallel and series resonances have a major influence on the frequency-dependent impedance $\underline{Z}(\omega)$.

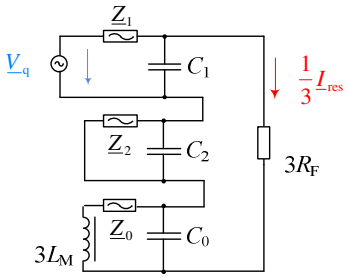

Figure 2: Equivalent earth-fault circuit

This becomes clear after transformation in the symmetrical components.

1) named after its inventor, PETERSEN W., 1880 - 1946

The equivalent circuit in Figure 2 shows directly the effective parallel resonance circuits in the positive ($\underline{Z}_1$), negative ($\underline{Z}_2$) and in the zero sequence ($\underline{Z}_0$) components. In addition series resonances circuits are formed between the positive/negative and the zero sequence components. All elements of the network are implemented in the symmetrical impedances $\underline{Z}_1$, $\underline{Z}_2$ and $\underline{Z}_0$. In Figure 2, the impedances are simplified to lumped elements. Overhead lines and cables have wave propagation characteristic which leads to natural frequencies $f_{e(W)}$. These natural frequencies can be considered (DRUML [5], SCHMIDT ET AL [6]) with a representation in two-port network with distributed elements, shown in Figure 3.

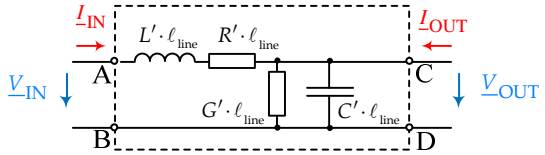

Figure 3: Two-port equivalent with distributed elements of a line segment

The complete behaviour of lines can be defined using equation (6):

$$\begin{bmatrix} \underline{V}_{IN} \\ \underline{I}_{IN} \end{bmatrix} = \begin{bmatrix} \cosh\left(\underline{\gamma} \cdot \ell_{line}\right) & \underline{Z}_w \cdot \sinh\left(\underline{\gamma} \cdot \ell_{line}\right) \\ 1/\underline{Z}_w \cdot \sinh\left(\underline{\gamma} \cdot \ell_{line}\right) & \cosh\left(\underline{\gamma} \cdot \ell_{line}\right) \end{bmatrix} \cdot \begin{bmatrix} \underline{V}_{OUT} \\ \underline{I}_{OUT} \end{bmatrix} \quad (6)$$

with the surge impedance $\underline{Z}_w$:

$$\underline{Z}_w = \sqrt{\frac{R' + j\omega \cdot L'}{G' + j\omega \cdot C'}} \quad (7)$$

and the complex propagation constant $\underline{\gamma}$:

$$\underline{\gamma} = \sqrt{\left(R' + j\omega \cdot L'\right) \cdot \left(G' + j\omega \cdot C'\right)} \quad (8)$$

The coefficient matrix in equation (6) can be defined as the transfer matrix $\underline{A}$. The advantage of the representation of lines by two-port parameters is the simple connection of several lines to an equivalent impedance in the respective component system. The transfer matrices of lines in series shown in Figure 4 can be multiplied to $\underline{A}_{12} = \underline{A}_{line1} \cdot \underline{A}_{line2}$.

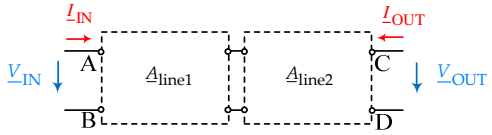

Figure 4: Lines in series

The transfer matrices of lines in parallel, shown in Figure 5, can be solved by adding the corresponding admittance matrices $\underline{Y}_{12} = \underline{Y}_{line1} + \underline{Y}_{line2}$. The back-transformation to the A-matrix representation leads to the transfer matrix $\underline{A}_{12} = \underline{Y}_{12}^{-1}$. Loads can be characterized by a series connection of a line and the load (see equation (9)).

$$\underline{A}_{load} = \begin{bmatrix} 1 & 0 \\ 1/\underline{Z}_{load} & 1 \end{bmatrix} \quad (9)$$

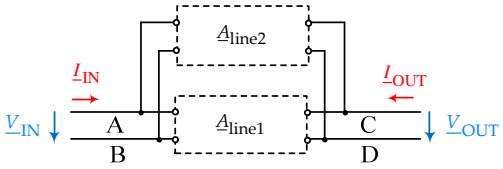

Figure 5: Lines in parallel

The transfer matrices of lumped shunt elements (transformers, PETERSEN coils) are represented by equation (10).

$$\underline{A}_T = \begin{bmatrix} 1 & \underline{Z}_T \\ 0 & 1 \end{bmatrix} \quad (10)$$

The losses of the lumped elements are considered. The equivalent configuration of a stub lines consisting of $\underline{A}_{line3}$ and f $\underline{A}_{load}$ is shown in Figure 6 and can be summarized to a new two-port $\underline{A}_S$ in between $\underline{A}_{line1}$ and $\underline{A}_{line2}$.

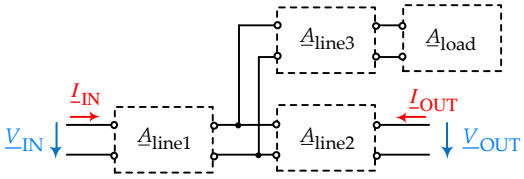

Figure 6: Stub line configuration

For the resulting two-port can be written $\underline{A}_{12} = \underline{A}_{line1} \cdot \underline{A}_S \cdot \underline{A}_{line2}$ (WEI; [7]). After transformation into two-port parameters, all elements can connected to the circuit in the symmetrical components as shown in Figure 7.

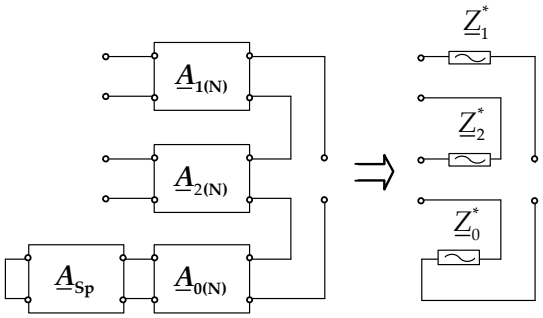

Figure 7: Resulting system in symmetrical components

The index (N) characterizes transfer matrices of network elements (lines, transformers), and the index (Sp) defines the parameters for the PETERSEN coil.

IMPLEMENTATION OF VOLTAGE AND CURRENT SOURCES

The calculation of the residual earth-fault current $\underline{I}_{res}$ is performed systematically. In the first step, the 50 Hertz part of the residual earth-fault current $\underline{I}_{res(50)}$ is calculated. It is possible to realize a simplified approach. The impedances in the zero-sequence system are very much larger than the impedances in the positive and in

the negative-sequence system. The circuit from Figure 2 can be reduced to Figure 8.

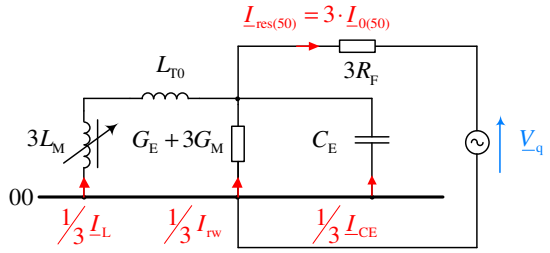

Figure 8: Simplified equivalent circuit for calculation of residual earth-fault current $\underline{I}_{res(50)}$

The calculation of current harmonics depends on the location of harmonic sources. It is assumed that the sources of the harmonics in the grid behave like current sources. It is required to measure the phase-to-earth harmonic voltage levels in the investigated system. The measured voltage harmonics (index ν(m)) are transformed into the symmetrical components. These harmonic voltages $\underline{V}_{\nu(m)}$ are then converted in current sources at the specific source location. In Figure 9 an example for the implementation of possible harmonic current sources in the positive-sequence system is shown. The frequency-dependent grid impedance $\underline{Z}_{1(G)}$ is additionally considered. This impedance represents the grid in front of the power transformers.

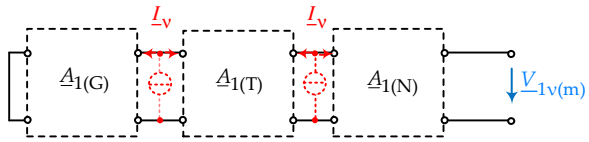

Figure 9: Implementation of possible harmonic equivalent current sources based on the measured harmonic voltages $\underline{V}_{1m}$

The same procedure as shown in Figure 9 is carried out for the negative-sequence and the zero-sequence system. However, it is difficult to define the correct location for the implementation of the converted harmonic current sources.

MEASUREMENTS OF RESIDUAL EARTH-FAULT CURRENTS

The results of field test were used for the verification of the model. The measurements were realized in a 20 kV-network, shown in Figure 10.

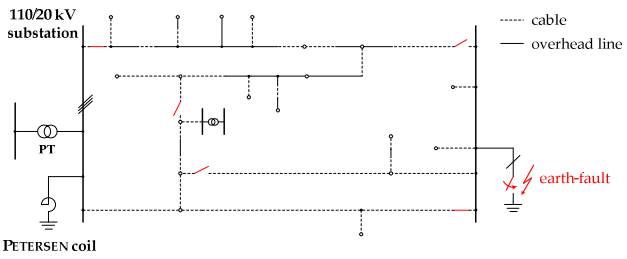

Figure 10: Single line diagram of the 20 kV-network

The length of the overhead lines in the network is approximately 20 % of total length. The measured capacitive line-to-earth current was determined to $I_{CE} \approx$ 115 A. The measurements contain the residual earth-fault currents, the harmonic currents and harmonic voltages under varying conditions. The RMS-value of the measured residual earth-fault current depends strongly on the failure resistance R_F. For the failure resistance $R_F \approx$ 0 Ω, the residual earth-fault current is depicted in Figure 11.

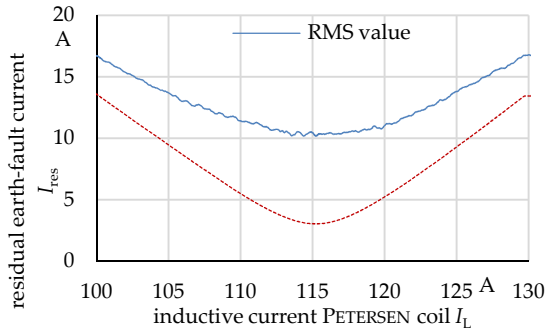

Figure 11: Measured residual earth-fault current in dependence on the inductive current $\underline{I}_L$ *for* $R_F = 0$

The waveform of the residual earth-fault current i_{res} at the resonant point is shown in Figure 12.

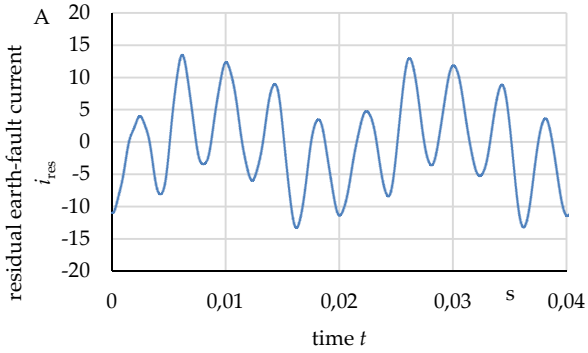

Figure 12: Measured waveform of residual earth-fault current with detuning factor $v \approx 0$ *and* $R_F = 0$

The harmonic voltages were measured in the fault case and in the pre-fault case.

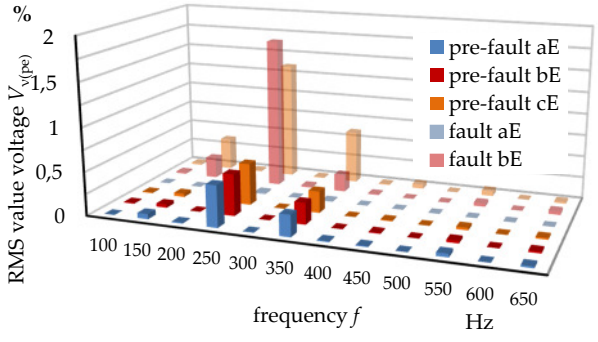

Figure 13: Measured phase-to-earth harmonic voltages $V_{\nu(pe)}$ *at the fault location*

The measured phase-to-earth (Index pe) voltages are shown in Figure 13.

CALCULATION OF RESIDUAL EARTH-FAULT CURRENTS

The parameters of the 20kV-network were extracted from the data base of the system operator. The concentrated parameters of the network are given in Table 1.

Table 1: Specific parameters of the 20 kV-network ($v = 0$)

Parameter	value
Transformer inductance ($L_T = L_{1(T)}$)	7 mH
Inductance zero-sequence ($L_0 = L_{0(Sp} + L_{0(N)}$)	1,13 H
Capacitance positive-sequence (C_1)	7,6 µF
Capacitance zero-sequence ($C_0 = C_E$)	8,2 µF

Saturation effects in the transformer and in the PETERSEN coil are neglected. The losses of the PETERSEN coil were based with 1.5 % of the rated reactive power (Q_r = 2 Mvar). The conductances of lines are shown in Table 2.

Table 2: Conductances of lines

Line		conductance
20 kV-overhead line	$G'_{E(ohl)}$	15 nS/km
20 kV-XLPE cable	$G'_{E(c)}$	6 nS/km

For the correct frequency-dependent model were the 20 kV-network reduced to two-pole sections. The sections are shown in Figure 14.

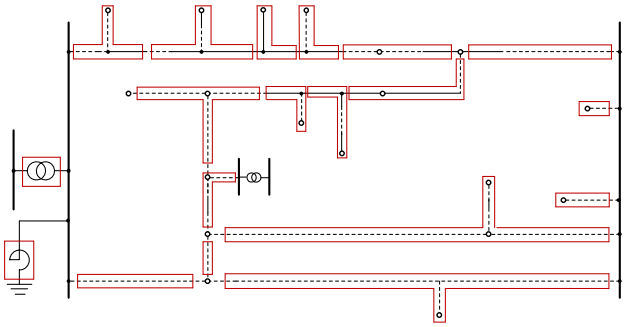

Figure 14: Sections of two-port network

The current harmonics in the residual earth-fault current and the frequency-dependent impedance $\underline{Z}(j\omega)$ depend strongly on the switching conditions in the network. The frequency-dependent impedances $\underline{Z}(j\omega)$ for different switching status (Figure 15) are shown in Figure 16.

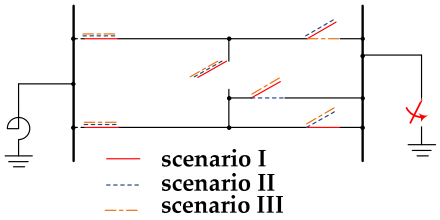

Figure 15: Switching status in the 20 kV-network

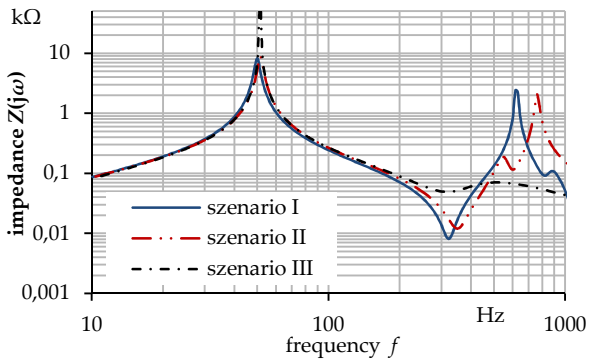

Figure 16: Frequency-dependent impedances of different switching configurations in the 20 kV-network

It is clear, that the switching status of the 20 kV-network must be considered. The typical switching status is depicted in Figure 10 (scenario I). The frequency-dependent impedance $\underline{Z}(j\omega)$ for earth-faults at the substation and the measurement location is shown in Figure 17. The dominated resonances frequency becomes clear in the diagram. The first parallel resonance is effective in the zero-sequence system ($f_{e(p)} \approx 50$ Hz), SCHMIDT ET AL [6].

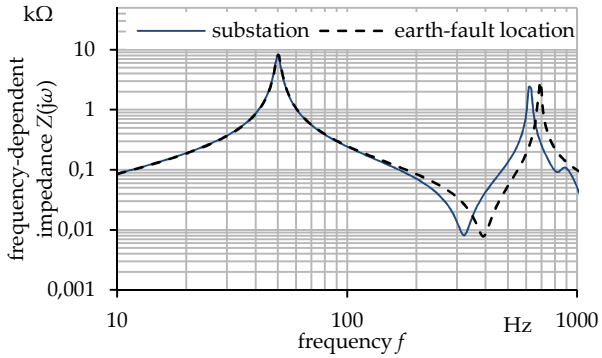

Figure 17: Frequency-dependent impedance $\underline{Z}(j\omega)$ at the substation and at the earth-fault location

The second parallel resonance in the positive-sequence system depends on the location of the earth-fault. The series resonance is evident for the level of the current harmonics in this area. The natural frequency for the series resonance can be estimated by equation (11).

$$f_{e(s)} = \frac{1}{2 \cdot \pi} \cdot \sqrt{\frac{L_0 + 2L_1}{2L_1 \cdot L_0 \cdot C_E + L_1 \cdot L_0 \cdot C_1}} \qquad (11)$$

In the 20 kV-network (Figure 10) the natural frequency is specified to $f_{e(s)} \approx 390$ Hz. This frequency conforms the substation busbar value given by Figure 17. In the specific network, the dominated resonance is determined in the area of the 5th and the 7th harmonic. Therefore, it was expected larger proportions for the 5th and 7th current harmonics. In the calculation they are investigated with current sources in the 20 kV- and in the 110 kV-system. The pre-fault voltages (see Figure 13) are used for the calculation of the current sources. The results of the

calculation are represented in Figure 18.

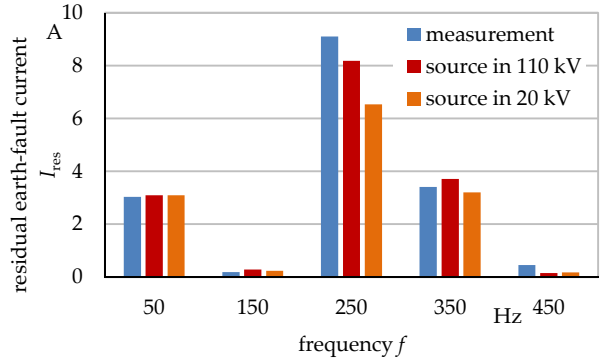

Figure 18: Comparison of the measured and calculated harmonic earth-fault current (two different locations of the harmonic current sources)

The best match between the measured and calculated current is accomplished with the assumption of harmonic current sources in the110 kV-network. This fact can be explained with the series resonances. From the 110 kV-side, the 20 kV-network has series resonances with a low impedance $\underline{Z}(j\omega)$. The inductances and the capacitances of the 110/20 kV-network plays an important role.

Table 3: Comparison of measured and calculated residual earth-fault currents $v = 0$

	measurement	calculation
Residual earth-fault current I_{res}	10,1 A	9,5 A
damping d	2,6 %	2,6 %

The comparison of the essential results are summarized in Table 3.

CONCLUSION

The harmonics in the residual earth-fault current I_{res} depends strongly on the network configuration. Higher harmonic currents occur from series resonances between the positive/negative-sequence and the zero-sequence impedances. The harmonic currents dominate the residual earth-fault current I_{res}.

The 20 kV-network can builds a series resonance with a low impedance $\underline{Z}(j\omega)$. If the resulting resonance is near to a characteristic harmonic, high harmonic currents via the fault location are possible.

A simple and good estimation of the residual earth-fault current I_{res} can be realized with the two-port models. The two-port models includes also the frequency-dependent behaviour of the network elements.

It is necessary to consider the switching status in the investigated network. The switching status has an important influence on the residual earth-fault current I_{res} in some scenarios.

Pre-fault harmonic voltages cannot be used for the implementation of sources voltages in the symmetrical component model because, higher harmonic currents will be effective by the series resonances and high harmonic voltages are effective by parallel resonances. Therefore, it is necessary to consider the frequency-dependent impedances $\underline{Z}(j\omega)$.

In the future, the influence of the frequency-dependent impedance $\underline{Z}(j\omega)$ of the 110 kV-system must be proven. Moreover the frequency-dependent parameters of cables and overhead lines are considered.

Acknowledgments

The authors thanks the colleagues with the KNG-Kärnten Netz GmbH and the KELAG for the help and the endorsement of this article.

REFERENCES

[1] PIETZSCH H., PRINZ S.;
Oberschwingungsanteile in MS-Netzen mit Erdschluss-Kompensation;
Proceedings, Energietag Brandenburg, Technical University Cottbus, 2008

[2] SCHWARZ J.;
Untersuchung der Einflussgrößen auf den Erdschlussreststrom in kompensierten Mittelspannungsnetzen und Beurteilung alternativer Verfahren zur Sternpunktbehandlung;
Diploma Thesis, FH Braunschweig/Wolfenbüttel, 2004

[3] STADE A.;
Erdschlussströme in MS-Netzen mit Resonanzsternpunkterdung;
etz, VDE-Verlag, 2011

[4] FISCHER M.;
Oberschwingungen im Erdschlussreststrom des kompensierten Drehstromnetzes;
Dissertation, University Stuttgart, 1981

[5] DRUML G.;
Innovative Methoden zur Erdschlussortung und Petersen-Spulen Regelung;
Dissertation, Technical University Graz, 2012

[6] SCHMIDT U., SCHEGNER P.;
Einfluss des Fehlerortes auf den Erdschluss-Reststrom bei Resonanz Sternpunkterdung im 110-kV-Netz;
Proceedings, ETG-Fachtagung Sternpunktbehandlung, Nürnberg, 2014

[7] WEI YU.;
Bestimmung des Erdschluss-Reststromes eines 20 kV-Netzes bei Berücksichtigung der Netztopologie und der Oberschwingungspegel;
Master Thesis, Technical University Dresden, 2014